Adaptive algorithm for gait segmentation using a single IMU in the thigh pocket

Francisco A. Garcia, Juan C. Pérez-Ibarra,
Marco H. Terra, *Member, IEEE*, and Adriano A. G. Siqueira, *Member, IEEE*

***Abstract*— Gait segmentation may help monitoring the evolution of patients during rehabilitation treatment through the analysis of properly defined metrics. Many algorithms detect gait events using Inertial Measurement Units (IMUs). However, most of them require the IMUs to be attached to the body, or to assistive devices. Often individuals must go to a gait laboratory which owns specialized equipment so that gait analysis can be performed. IMUs are present in modern smartphones. An IMU/smartphone carried in the pocket during daily activities could allow the analysis of much more data in a more comfortable setting. We address the detection of four gait events: Heel-Strike (HS), Flat-Foot (FF), Heel-Off (HO) and Toe-Off (TO) using a single noisy IMU attached to a smartphone placed inside the thigh pocket. Gait was modelled as a four-state left-right Hidden Markov Model (HMM) whose observations follow multivariate Gaussian distributions. The decoding in post-processing was performed with a modified Viterbi decoder that accounts for a rule-based (RB) detection of TO. To validate the approach, experiments were performed in nine subjects with no gait abnormalities. Our algorithm obtained median F1-Scores $\geq$ 0.955 for all events in intra-subject evaluation and median F1-Scores $\geq$ 0.757 in inter-subject evaluations (with fast training and with a populational model). It demonstrated high generalization capability in our dataset and competitive performances when compared to other algorithms using high-quality IMUs attached to the body. This work is a step towards accurate and refined gait segmentation using a smartphone carried in the pocket.**

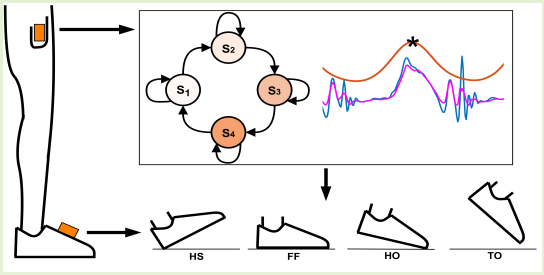

***Index Terms*— Gait analysis, hidden Markov model, inertial measurement units, machine learning, wearable sensors.**

I. Introduction

GAIT segmentation refers to the process of dividing the human gait cycle into phases that indicate changes in the foot-ground dynamics. Gait events are time instants where transitions between those phases occur. Detection of these events is possible through algorithms that process gait signals allowing gait segmentation to be performed automatically.

Gait segmentation has many applications in gait analysis for physical therapy and rehabilitation. For example, metrics derived from the event detection may indicate the degree of gait impairment [1], which could help monitoring the evolution of patients during rehabilitation treatment. Many types of sensors have been utilized to capture gait data [2]. Usually considered gold standards include footswitches, foot pressure insoles, force platforms and optoeletronic systems. The first two have short service life, while the last two are only suitable for indoor applications at specialized gait laboratories [3].

Inertial Measurement Units (IMUs) have become increasingly attractive because they are cheap, durable, mobile, reliable [2] and present in modern-day smartphones. Previous algorithms for gait segmentation using IMUs achieved high performances for the foot, shank [2] and thigh [4] locations. However, most of them require the IMUs to be attached either to the body by straps, or to another device, such as exoskeletons or adapted shoes.

Since smartphones contain IMUs and are often carried in the thigh pocket, accurate detection of gait phases using a single IMU inside a trouser/skirt/shorts pocket could bring new applications for gait analysis, such as continuous monitoring of patients in rehabilitation treatment. Much more data from natural daily activities could be analysed, contrarily to gait laboratory settings which are more artificial and limited data can be acquired [5].

Therefore, we address here the problem of detecting four gait events: Heel-Strike (HS), Flat-Foot (FF), Heel-Off (HO) and Toe-Off (TO) using a single noisy IMU placed inside the thigh pocket.

II. Background

Manuscript received ...; revised ... This study was supported in part by the Coordenação de Aperfeiçoamento de Pessoal de Nível Superior - Brasil (CAPES) under Finance Code 001 and grant PNPD-88887.368451/2019-00; in part by São Paulo Research Foundation (FAPESP) under grants 2011/10369-6 and 2013/14756-0.

(Corresponding author: Francisco A. Garcia.)

Francisco A. Garcia, Juan C. Pérez-Ibarra and Marco H. Terra are with the Department of Electrical Engineering, University of São Paulo, São Carlos 13566-590, Brazil. (emails: franc.ambr10@gmail.com; jcperez-ibarra@sc.usp.br; terra@sc.usp.br). Adriano A. G. Siqueira is with the Dept. of Mechanical Engineering, University of São Paulo, São Carlos 13566-590, Brazil. (email: siqueira@sc.usp.br)

A. Gait phases

Human gait is a cyclic pattern [6] that has been segmented from two to eight phases in the literature [3]. Gait events correspond to the transitions between phases, therefore gait segmentation and detection of gait events are equivalent problems. The majority of the existing approaches to detection of gait events include at least the two events: Heel-Strike (HS), when the foot first touches the floor, also denominated Initial Contact (IC), and Toe-Off (HS), when the foot loses contact with the floor, also denominated End Contact [7]. We consider two more events: Flat-Foot (FF), when the complete sole of the foot contacts the floor, and Heel-Off (HO), when the heel loses contact with the floor. Although the pattern HS-FF-HO-TO is usually observed in normal gait, it may vary in pathological gait. The gait phases are then defined as the time interval between two subsequent events, as shown in Fig. 1.

B. Previous approaches

Algorithms for detection of gait events may be split into machine learning-based or rule-based. Learning-based methods have the advantage of not requiring careful hand tuning of parameters nor the knowledge of specific characteristics of the signals used to detect the events. They may grasp patterns and relations between signals and gait events that would be imperceptible even to human experts. Examples include Hidden Markov Models (HMMs) [8], [9], Genetic Algorithms [10], Gaussian Mixtures [11], Decision Trees [12] and Neural Networks [13].

Rule-based approaches assume that gait events occur when input signals match a set of rules, which are often defined by a specialist. They have the advantage of being interpretable, very simple to implement and frequently suitable to online applications because low computational power is required. For example, [4] is based on the search of a min-max-min sequence in the sagittal angular velocity of the shank.

Many algorithms are capable of accurately detecting gait events in healthy [2], [14] and recently in impaired subjects [10], [15] using IMUs attached to the foot, shank and thigh. The classification accuracy of four gait phases in [13] was (97.2±0.8)% using thigh-only signals acquired from a 3D motion capture system. In [16], 98.9% of the HS and TO events were recognized using an IMU attached on the thigh area of a wearable device. These works often assume that the gait cycle is segmented into a finite number of states.

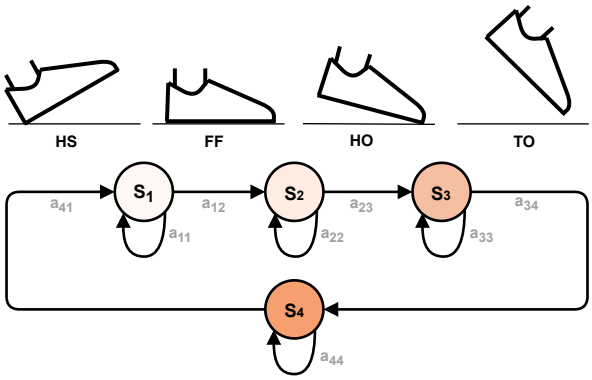

Fig. 1. Human gait modelled as a HMM with four states. The transitions to subsequent states happen when a gait event is detected (HS, FF, HO, TO). The cyclic pattern in usual gait is enforced on the model's structure. a_{ij} is the transition probability from state S_i to state S_j. HMM diagram redrawn from [8].

Instead of discretizing the gait cycle, another approach to gait segmentation consists of finding a continuous correspondence between the gait cycle and a so-called phase variable. Several studies obtained promising results using this technique. In [17]–[19] , the authors showed that the thigh - or hip - angle, possibly along with its integral or derivative can accurately track human gait cycle. They used motion capture cameras in [18] and an IMU attached to a prosthetic limb in [17], [19]. In [20], the gait phase estimation error on slow walking was 1.67±1.36% using a LSTM-based neural network using inputs from IMUs attached to the thigh and torso.

Smartphones, often carried in the thigh pocket, have already been employed to gait analysis because they contain sensors such as GPS, microphone, cameras and IMUs. Common applications include activity recognition [21], energy expenditure estimation, fall detection, step counting, pedestrian tracking [22], user authentication [23] and monitoring of medicine intake [24]. Many of the current approaches rely on machine learning, for example to: 1. classify the signals on an activity category (e.g. walking, running, etc...) [21], 2. identify an user [23] or 3. infer whether a patient is following the treatment [24]. Other methods are able to quantify gait features such as gait velocity [25], step frequency, step length and step cycle regularity [26], which may for example be used to characterize Parkinson's gait [27]. These techniques may be based on frequency domain, time domain analysis or both [24].

Detection of gait events plays an essential role in time domain analysis, since the events may be used to calculate gait features over time. Although important features such as the aforementioned ones can already be estimated by the existing methods, they currently do not allow a refined description of the gait cycle, since their segmentation algorithms are intended to identify the entire cycles (e.g. [24], [28]). A finer segmentation is relevant, for example, to detect a longer flat-foot phase that is associated with metabolic inefficiency [29]. In this direction, the authors in [30] discussed the suitability of fine-grained gait segmentation using an IMU in the thigh pocket, but an algorithm was not proposed. In [31], the authors introduced a generic approach to detect user-defined points from any IMU/smartphone positioning, but the performance was only tested for the shoe-mounted location.

In an attempt to overcome the current lack of algorithms for accurate and refined gait segmentation using an in-the-pocket IMU/smartphone, we present here a method to detect four gait events using a single noisy IMU in the thigh pocket (section III). Our method is an unifying approach between HMM-based and rule-based algorithms that combines ideas from:

1) Machine learning-based approach from Mannini et al., (2011) [9]: They modelled human gait as a four-state left-right HMM (Fig. 1) whose hidden states are the gait phases and the corresponding observations are the sagittal angular velocity of the foot captured by a single foot-mounted gyroscope. The

gait phases were decoded in post-processing using the Viterbi algorithm. In [8], the authors made an online implementation.

2) Rule-based approach from Piriyakulkit et al., (2017) [16]: They detected three gait events (HS, TO, and Terminal-Swing) using the sagittal angular velocity and the forward linear acceleration of the thigh from an IMU placed on an assistive device on the side of the leg. The algorithm requires hand-tuning of 9 parameters (2 filters, initialization of 3 windows, 3 thresholds and 1 window length). They considered a negative angular velocity and a positive linear acceleration when the leg is going forward.

- TO is detected when the filtered angular velocity achieves a local minimum below an adaptive threshold.
- Terminal Swing occurs when the filtered angular velocity achieves a local maximum above an adaptive threshold.
- HS point corresponds to the local maximum above an adaptive threshold of the filtered linear acceleration.

In the next section we describe our proposed algorithm to detect four gait events using an IMU in the thigh pocket.

III. Methods

A. Modeling Human Gait using a Hidden Markov Model

We model human gait as a discrete-time, four states $S = \{S_1, S_2, S_3, S_4\}$ left-right HMM as in [9], (Fig. 1). It mathematically represents the idea that we do not have direct access to the actual gait phases (or states), but rather to observations derived from the sensor measurements that are related to the corresponding hidden gait phases. The sequence of hidden states is denoted by $Q = \{q_1, ..., q_N\}$, where N is the number of time instances in the data series. We adopt the same notation used in [32].

The transition probabilities $a_{ij} = \mathbb{P}\{q_{n+1} = S_j | q_n = S_i\}$, $n \in \{1, ..., N\}$, from state S_i to state S_j are arranged in the transition probability matrix $\mathbf{A} = [a_{ij}]_{(S_i,S_j)\in S^2}$. Assuming that human gait is a cyclic pattern going uniquely in the forward direction, $\mathbf{A}$ has non-zero terms only on the main diagonal and on the diagonal immediately above:

$$\mathbf{A} = \begin{bmatrix} a_{11} & a_{12} & 0 & 0 \\ 0 & a_{22} & a_{23} & 0 \\ 0 & 0 & a_{33} & a_{34} \\ a_{41} & 0 & 0 & a_{44} \end{bmatrix} \quad (1)$$

At each time instance t_n we assume to have access to the observation $\boldsymbol{O}_n$, which is a vector in $\mathbb{R}^{\mathbb{N}}$ composed of signals derived from an IMU in the thigh pocket.

We assume that the observations associated to each state $S_{i\in\{1,...,4\}}$ follow a multivariate Gaussian distribution with mean vector $\boldsymbol{\mu}_i$ and covariance matrix $\boldsymbol{\Sigma}_i$. This assumption is a generalization of previous works which modelled the observations as a univariate Gaussian distribution [8], [9]. The probability distributions of the observations are arranged in the observation vector:

$$\mathbf{B} = \left\{ b_{i\in\{1,...,4\}} = \mathcal{N}(q_n | \boldsymbol{\mu}_i, \boldsymbol{\Sigma}_i, q_n = S_i) \right\} \quad (2)$$

The model λ is fully described by 3 parameters: $\lambda = (\boldsymbol{\pi}, \mathbf{A}, \mathbf{B})$, where $\boldsymbol{\pi} = [0.1, 0.4, 0.1, 0.4]$ is the prior probabilities vector, which we take as an approximate probability distribution of the four states.

B. Modified Viterbi decoder and TO-Rule

Having the model λ and a sequence of observations $\boldsymbol{O} = \{\boldsymbol{O}_1, ..., \boldsymbol{O}_N\}$, the sequence of hidden states $Q^* = \{q_1^*, ..., q_N^*\}$ that optimally explains the observations in the data series can be estimated efficiently by the Viterbi algorithm. It finds the maximum likelihood state sequence and is composed of two main steps: In the first step, a forward pass over the data points calculates the partial likelihood (score) of the most probable path ending at each state at each time instance. A matrix of back-pointers is constructed indicating the most probable previous state of each possible state at time step t_n. In the second step, a backtracking is performed over the back-pointers to find the most probable path [8]. We adopted log probabilities to avoid numerical problems [32].

In addition, we observed that the pure HMM in Fig. 1 decoded by the standard Viterbi algorithm has a major weakness in detecting TO using data from an IMU in the thigh pocket. Therefore we designed a TO-Rule based on [16]. We consider that TO event corresponds to a local maximum of the signal $\overline{\omega}_s$, which is the sagittal angular velocity of the thigh ω_s (here positive when the leg is going forward) once filtered and normalized (section IV). ω_s is captured by the IMU located in the thigh pocket. The local maximum in $\overline{\omega}_s$ is detected as a change in the signal of its derivative $\alpha = \frac{d\overline{\omega}_s}{dt}$, which is estimated using the first-order finite difference of $\overline{\omega}_s$.

The standard Viterbi decoder was modified in order to detect TO using this rule. During the forward pass step, our algorithm is identical to the standard Viterbi decoder. During the backtracking step, TO event is detected by TO-Rule regardless of the backward pointers. Our algorithm allows the incorporation of expert knowledge through rules that may be added into the decoding. However, by doing this, the optimal state sequence in the criterion of maximum likelihood is no longer ensured.

The main steps of the algorithm are shown in Algorithm 1. Additional minor steps can be found in [32]. Note that since the backtracking runs in the opposite direction of the time instances, TO event is characterized by a transition from S_4 to S_3 in the TO-Rule. It was implemented in MATLAB based on the HMM Toolbox [33].

IV. Observation vector

In this section we present signals used as observations for HMMs. In addition to the proposed approach which considers signals derived from the IMU in the thigh pocket, we evaluated several HMMs with different inputs from different sensor placements. We also compared the results with some algorithms taken from the literature. Signals used as inputs to algorithms from the literature were filtered according to the original works.

A. Filtering

The signals used in this study as observations were filtered with second order butterworth filters that are applied forwards and backwards, according to Table I, where a means acceleration and ω angular velocity.

Algorithm 1 Modified Viterbi decoder

Forward pass :
for $n \leftarrow 1, ..., N$ **do**
  for all $S_j \in S$ **do**
    $\delta_n(j) \leftarrow \max_{S_i \in S} \{\delta_{n-1}(i) + \log[a_{ij}])\} + \log[b_j(\boldsymbol{O}_n)]$
    $\psi_n(j) \leftarrow \arg\max_{S_i \in S} \{\delta_{n-1}(i) + \log[a_{ij}])\}$
  end for
end for
Modified backtracking :
for $n \leftarrow N-1, ..., 1$ **do**
  if $q^*_{n+1} = S_4$ **then**
    $q^*_n \leftarrow$ TO-RULE(α, n)
  else
    $q^*_n \leftarrow \psi_{n+1}(q^*_{n+1})$
  end if
end for

function TO-RULE(α, n)
  if $\alpha_n \geq 0 \wedge \alpha_{n+1} < 0$ **then**
    return S_3 ▷ TO detected (Local maximum of $\overline{\omega}_s$)
  else
    return S_4 ▷ Waiting for detection of TO
  end if
end function

TABLE I
SIGNALS USED FOR HMMS AT DIFFERENT SENSOR PLACEMENTS

IMU Location	Signals	Lower cut-off frequency (Hz)	Higher cut-off frequency (Hz)
Foot-mounted [9]	ω_s	-	15
Shank-attached	ω_s	-	15
Thigh-attached	ω_s	0.2	1.5
Pocket	ω_s	0.2	1.5
Pocket	$\omega_{x,y,z}$, $a_{x,y,z}$	0.2	15

z: Vertical axis. y: Anterior-posterior axis. x: Medio-lateral axis. ω_s: sagittal angular velocity.

The low-pass filter parameter (15 Hz) for the foot was taken from previous literature [9]. Since the amplitude spectra of gait signals is concentrated below 15 Hz [34], this cut-off frequency was also used for shank-attached and some pocket signals. In addition, based on discussions in [35], we found that including the thigh-attached and pocket ω_s signals filtered at 1.5 Hz significantly improved the results. This filter extracts the fundamental component of the gait, which is usually below 1.4 Hz for fast walking when the walking frequency is measured from a single leg [34], [36], [37]. We also removed low frequency components (below 0.2 Hz) to reduce slow drifts in inertial sensors [38] and to make our algorithm invariant to constant biases. The thigh-attached IMU was only used for comparison, since our interest lies on the pocket location. Note in Table I that ω_s and ω_x pocket signals are derived from the same output (gyro in the medio-lateral direction), but filtered at different frequencies. The resultant angular velocity ω_r is calculated using the filtered ω_x, ω_y and ω_z:

$$\omega_r = \sqrt{\omega_x^2 + \omega_y^2 + \omega_z^2} \tag{3}$$

Similarly for the resultant linear acceleration a_r:

$$a_r = \sqrt{a_x^2 + a_y^2 + a_z^2} \tag{4}$$

Finally, ω_r and a_r are filtered with band-pass filters with pass-band of [0.2, 1.5] Hz. This additional filter removes components originated from the squaring operation. From now on, filtered signals are denoted with a tilde (e.g. $\tilde{\omega}_s$). Note that all filter parameters are given, therefore the algorithm does not need subject-specific tuning of filters.

B. Adaptive normalization

After being filtered according to the previous section, the thigh signals were normalized in an adaptive fashion as follows. Let $\tilde{s}(n)$ be the filtered signal at time instance n and $W(n) = [\tilde{s}(n-k), ..., \tilde{s}(n), ..., \tilde{s}(n+k)]$ a sliding window centered at $\tilde{s}(n)$ with length $(2k+1)$ corresponding to 2.5 s. This length was chosen to be larger than one stride for slow gait considering all prediction intervals in [36], which is the scenario where the stride has the largest duration. This parameter does not need to be tuned since it is based on population statistics. The normalized signal $\bar{s}(n)$ at time instance n is given by Eq. 5:

$$\overline{s}(n) = \frac{\tilde{s}(n) - \min(W(n))}{\max(W(n)) - \min(W(n))} \tag{5}$$

C. Observation

In our algorithm we defined the observation vector as:

$$\boldsymbol{O}_n = [\overline{\omega}_s(n), \overline{\omega}_r(n), \overline{a}_r(n)]^T \tag{6}$$

We tested several different combinations of outputs using data from a single subject and these are the variables that provide the best results.

D. Gold standard

Since the usually considered gold standards (e.g. pressure sensors and optoeletronic systems) were not available in our dataset, we adopted a set of rules using a foot-mounted IMU to be gold standard, based on the rules presented in [9].

New rules were added in order to make the original rules in [9] more robust to artifacts and to the variability of gait patterns among individuals. Our gold standard is presented in the following.

Let $a_{z_{foot}}(n)$ and $\omega_{foot}(n)$, $n \in \{1, ..., N\}$ be the raw signals of the vertical acceleration and the sagittal angular velocity of the foot, respectively. First, a pre-processing of $\omega_{foot}(n)$ substitutes points having an absolute value greater than 1200°/s by the linear extrapolation of their two predecessors, since we found by visual inspection that two points in our entire foot dataset were on the extremes of the IMU scale (±1500°/s). This is way beyond the normal range for gait data and is likely due to errors on the IMU.

Then, let $\tilde{\omega}^{F;O}_{foot}(n)$ be $\omega_{foot}(n)$ filtered by a butterworth low-pass filter with cutoff frequency F (given in Hz) and order

O which is applied forwards and backwards. The gold standard events are detected in sequence according to the following rules:

- FF: $|\tilde{\omega}_{foot}^{15;2}(n)| \leq \lambda_{FF} \wedge \frac{d\tilde{\omega}_{foot}^{5;10}(n)}{dt} > 0$
- HO: $|\tilde{\omega}_{foot}^{15;2}(n)| > \lambda_{HO} \wedge \frac{d\tilde{\omega}_{foot}^{3.5;2}(n)}{dt} < 0$
- TO: $\tilde{\omega}_{foot}^{15;2}(n-1) \leq 0 \wedge \tilde{\omega}_{foot}^{15;2}(n) > 0$
- HS point t_{HS} is found by Algorithm 2, where t_{TO} is the last TO point and L is a searching window length corresponding to 0.1 s

where $|.|$ denotes the absolute value, $\lambda_{FF} = \lambda_{HO} = 50°/s$ [9] and $t_{hyst} = 0.1$ s is a temporal hysteresis that does not allow the swing phase to last less than 0.1 s, which is reasonable since the swing phase corresponds to approximately 40% of the gait cycle [6].

Algorithm 2 HS algorithm for gold standard

1: **if** $\tilde{\omega}_{foot}^{15;2}(n) \leq 0 \wedge (t_n - t_{TO}) > t_{hyst}$ **then**
2: $\quad t_{HS} = \underset{n \leq i \leq n+L}{\arg\max}\, a_{z_{foot}}(n)$
3: **end if**

In [9], the rules are only based on the signal $\tilde{\omega}_{foot}^{15;2}(n)$. We added rules for FF and HO to ensure that FF occurs at the ascending part of the foot saggital angular velocity and HO on the descending part. As shown on the top pannel of Fig 2, small oscillations on the angular velocity can cause false detections by the original algorithm [9]. Therefore, we also consider the signal filtered at lower frequencies to overcome those oscillations. These filters were tuned by visual inspection of the foot dataset to correct cases in which [9] failed. Our HS rule differs from [9] since in our study the acceleration was available. As shown in Fig 2, the vertical acceleration of the foot has a distinct peak when HS occurs, which our algorithm starts to look for after the angular velocity has crossed zero to negative side.

Fig. 2 shows an example of signals acquired from the foot-mounted IMU and the corresponding states based on our rules (orange) and on the original rules in [9] (black).

V. Model Training

Given a sequence of training observations $\boldsymbol{O} = \{\boldsymbol{O}_1, ..., \boldsymbol{O}_T\}$ and the corresponding training gold standard states $G = \{g_1, ..., g_T\}$, where T is the number of training samples, the transition probability matrix $\mathbf{A}$ is estimated by:

$$a_{ij} = \frac{N_{strides}}{N|_{g_n=S_i}}, \quad j = i+1 \pmod 4 \tag{7}$$

$$a_{ii} = 1 - a_{ij}, \tag{8}$$

where $N_{strides}$ is the number of training strides and $N|_{g_n=S_i}$ the number of appearances of state S_i in the training gold standard sequence. Note that $N|_{g_n=S_i}$ depends on the sampling frequency. The conversion of a_{ij}^{f1} on frequency f_1 to frequency f_2 is: $a_{ij}^{f_2} = a_{ij}^{f_1} \cdot \frac{f_1}{f_2}$.

The parameters $\boldsymbol{\mu}_i$ and $\boldsymbol{\Sigma}_i$ are estimated as the sample average and the sample covariance matrix, respectively:

$$\boldsymbol{\mu}_i = \text{Avg}[\boldsymbol{O}_n|_{g_n=S_i}], \quad n \in \{1, ..., T\}, \quad i \in \{1, ..., 4\} \tag{9}$$

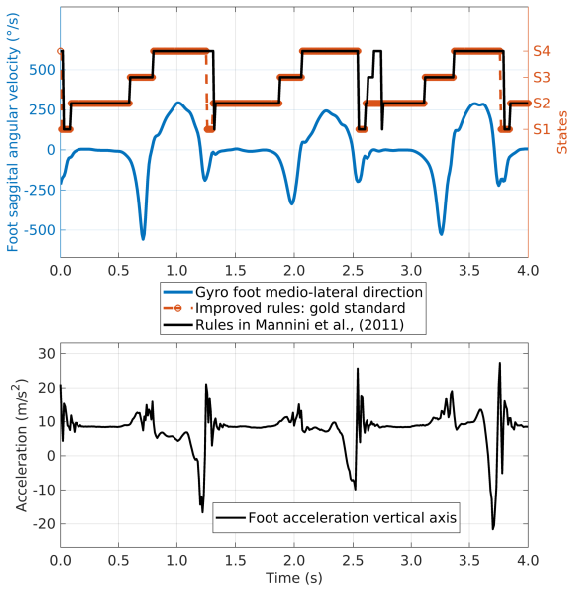

Fig. 2. Rule-based gold standard using the sagittal angular velocity (top) and the vertical acceleration (bottom) of the foot from a foot-mounted IMU. The improved rules are more robust to artifacts in comparison to the rules proposed by Mannini et al., 2011 [9]. Here, the HS detection corresponds to the positive peak in the vertical acceleration of the foot.

$$\boldsymbol{\Sigma}_i = \text{Cov}[\boldsymbol{O}_n|_{g_n=S_i}], \quad n \in \{1, ..., T\}, \quad i \in \{1, ..., 4\}, \tag{10}$$

where $\boldsymbol{O}_n|_{g_n=S_i}$ is the observation at time n so that the corresponding gold standard state is S_i.

VI. Experiments

In this section we describe the experiments that were conducted to validate our algorithm and the performance metrics that were computed. The results are then presented in comparison to other algorithms in the literature that were run on the same data.

The tests were approved by the ethics committee of the University of São Paulo, School of Physical Education and Sport of Ribeirão Preto, EEFERP-USP, CAAE #41150620.7.0000.5659, decision statement (approval) #4.579.836. The experiments were explained to the subjects and they provided informed consent prior to participation.

A. Experimental protocol

Nine subjects (7 males, 2 females, 23-59 years, 1.54-2.00 m, 57-92 kg, no gait abnormalities) performed three walking sessions at different speeds, either on a non-tilted treadmill or overground (8 treadmill, 1 overground). Walking sessions lasted 4.2±2.5 min. The subjects were asked if they wanted to rest for a few minutes between each walking session.

1) Treadmill: First, the subjects were asked to select the most comfortable walking speed (Self-Selected Walking Speed (SSWS)), then at 1.2·SSWS and finally at 0.8·SSWS. One of the subjects had two walking sessions at SSWS since the chosen SSWS was the lowest speed on the treadmill scale.

2) Overground: One of the subjects walked overground on a corridor instead of at the treadmill due to an unavailability of the treadmill on the test day. This subject was asked to walk first at Overground Self-Selected Walking Speed (OSSWS), then slightly faster than OSSWS and finally slightly slower than OSSWS, according to self perception of speed.

SSWSs varied from 1.0 to 4.5 km/h, with average±SD of 3.11±1.19 km/h. The total number of strides was 5074 (on average 188±129 per walking session), counted automatically as the number of TO events in the gold standard.

B. Experimental setup

Inertial data was captured at 100 Hz by Xsens MTw Awinda wireless IMUs. Data was transferred to a laptop (Intel® Core™ i5-8250U, 8 Gb RAM, Ubuntu 18.04) through the Awinda™ protocol which ensures data synchronization within 10 μs. The receiver station was kept close to the treadmill ($<$ 4 m). The subjects were asked to wear a trouser or shorts having a pocket either at the front or at the side of the thigh. Since our envisioned application is to perform gait segmentation using a smartphone, one Xsens IMU was attached to a smartphone (Moto G8 Power) by adhesive tape so that the Xsens IMU captured the movements of the smartphone. Then, the IMU-smartphone group was placed inside the thigh pocket on the dominant leg. The positioning of the pocket IMU-smartphone group was not readjusted between walking sessions in order to allow the natural change in orientation inside the pocket. It is important to remark that we only recorded and used data from the Xsens IMUs in this study.

One IMU was foot-mounted (gold standard), one was attached to the front of the shank, one attached to the thigh, all on the dominant leg (Fig. 3). The pocket, (shank and thigh)-attached IMUs were upright-oriented. The foot-mounted IMU was oriented on the logitudinal axis. The IMUs were attached to the body by velcro straps that come within the sensors kit. To avoid mechanical interference/contact from the thigh-attached IMU on the pocket IMU, the thigh-attached IMU was attached to the side of the thigh if the pocket was frontal and to the front of the thigh if the pocket was lateral.

C. Noise Simulation of Smartphone MEMS IMU

Since we only recorded data from the Xsens IMUs, we added simulated noises to the pocket Xsens signals in order to mimic the signal quality from a smartphone MEMS IMU. We considered two noise terms - bias instability (B) and angle/velocity random walk (N) - which often dominate in timescales varying from seconds to hours [39], [40].

We used parameters for the Honor Play smartphone (Huawei Technologies Co., Ltd.). The angle/velocity random walk was modelled as a white Gaussian random noise with power spectral density N^2 and the bias instability as a Gauss-Markov Error Model as in Eq. 11. For a detailed explanation on modeling IMU errors, we refer the reader to [41].

$$\dot{z}_G(t) = -\frac{1}{T_B} z_G(t) + \omega_B(t) \tag{11}$$

where $z_G(t)$ is the bias instability noise, T_B is the correlation time and $\omega_B(t)$ a white Gaussian noise with power spectral density $\frac{2B^2 ln(2)}{\pi(0.4365)^2 T_B}$. The parameters and their source are given in Table II.

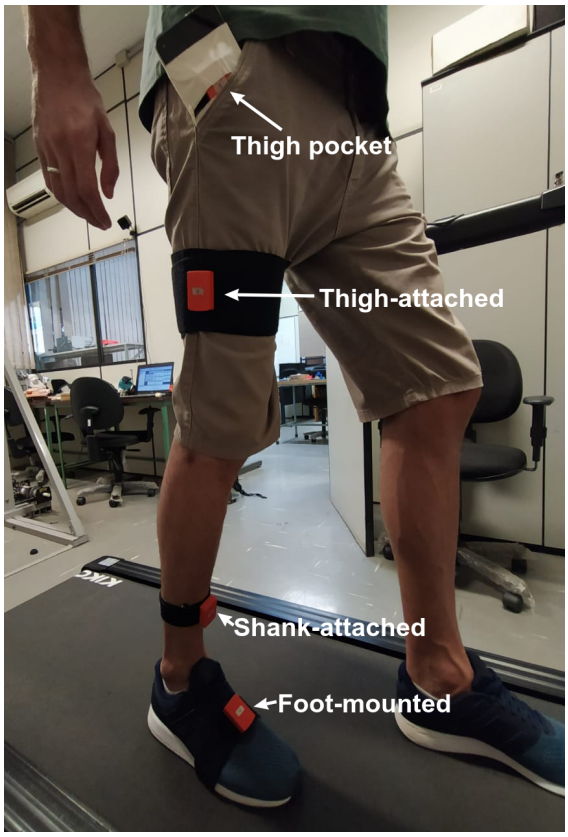

Fig. 3. Experimental setup: IMUs positioning to capture gait data. The foot-mounted IMU is used as reference. An IMU is attached to a smartphone placed inside the thigh pocket. The IMU-smartphone group is shown partially out of the pocket to facilitate visualization.

TABLE II
PARAMETERS FOR SMARTPHONE MEMS IMU NOISE SIMULATION

IMU Outputs	Bias instability (B) (mg) (°/s)	Noise density (N) (μg/$\sqrt{\text{Hz}}$) (°/$\sqrt{\text{h}}$)	Correlation time (T_B) (s)
Accelerometers	150	180	70
Gyroscopes	3	0.42	400

B and N parameters were taken from [42] and T_B from [43].

VII. PERFORMANCE EVALUATION PROTOCOL

The performance metrics that were computed and the three types of evaluation are described in the following.

A. Metrics

1) F1-Score: This metric is commonly used in the literature to evaluate event detection algorithms (e.g. [12], [15]). For each gait event, the $F1$-Score $\in [0, 1]$ is defined as the harmonic mean of Precision (P) and Recall (R): $\text{P} = \frac{\text{TP}}{\text{TP+FP}}$, $\text{R} = \frac{\text{TP}}{\text{TP+FN}}$, $F_1 = \frac{2 \cdot \text{P} \cdot \text{R}}{\text{P+R}}$, where TP are the True Positives, FP the False Positives and FN the False Negatives. TP are the first events correctly detected by an algorithm that lie within a tolerance window of ± 200 ms around the

corresponding gold standard events. FP are the detected events that lie outside the tolerance window or additional detections after a first correct detection. FN are the gold standard events that were not detected within the tolerance window. Higher $F1$-Scores are better.

2) Mean squared error (MSE): First we define the error between two states, corresponding to the minimum number of jumps between them in any direction:

$$error(S_a, S_b) = \begin{cases} 1, & \text{if } (a,b) \in \{(1,4),(4,1)\} \\ |a-b|, & \text{otherwise} \end{cases} \quad (12)$$

Let $G = \{g_1, ..., g_N\}$ be the gold standard state sequence and $Q = \{q_1, ..., q_N\}$ the sequence of hidden states found by an algorithm. The MSE of Q is:

$$\text{MSE} = \frac{1}{N}\sum_{n=1}^{N} error(g_n, q_n)^2 \quad (13)$$

Lower MSEs are better. This metric is very fast to compute and has the advantage that the delays in the decoded sequence degrade the final performance in a more continuous way than in the $F1$-Score. Of note, similar metrics have been utilized in the gait segmentation literature (e.g. [20], [44]).

B. Types

1) Evaluation 1 (Eval. 1) - Intra-subject: The model is trained with the first 20 s of one walking session performed by a subject and the performance is tested with the remaining data of the same subject (including the remaining data of the walking session used to train the model and the other two walking sessions). For each subject, this procedure is repeated 3-fold, using at each repetition the $n^{\text{th}} \in \{1,2,3\}$ walking session performed by the subject to train the model.

2) Evaluation 2 (Eval. 2) - Inter-subject, fast training: The model is trained with the first 20 s of one walking session performed by a subject and the performance is tested on the walking sessions performed by all the remaining subjects. This procedure is repeated using every walking session of every subject as the training data. Here we intended to test if it is possible to train the model fast with a single subject and apply the model in different subjects.

3) Evaluation 3 (Eval. 3) - Inter-subject, populational model: For each testing subject, (N-1) subjects are randomly picked with replacement from the remaining subjects. For each of the (N-1) picked subjects, 3 models are trained using the first 20 s of three walking sessions picked randomly with replacement. The final populational model is considered as the average of the (N-1)*3 randomly selected models. Note that the average of stochastic matrices is still a stochastic matrix. The same holds for the average of covariance matrices. This procedure is repeated 250 times for each testing subject. Here we evaluated how well the model performs when being trained with several subjects and being tested on an unseen subject.

Training data is never used in evaluation. We computed the $F1$-Score and the MSE at each testing walking session (3 per subject) for every cross-validation (Eval. 1 and 2) or pooling (Eval. 3) and we report the median and the interquartile interval [Q1 Q3] obtained for the metrics. In this manner it is possible to evaluate the repeatability of the performance. All analyses were run in post-processing on MATLAB R2018a. The start and end of each walking session were identified manually.

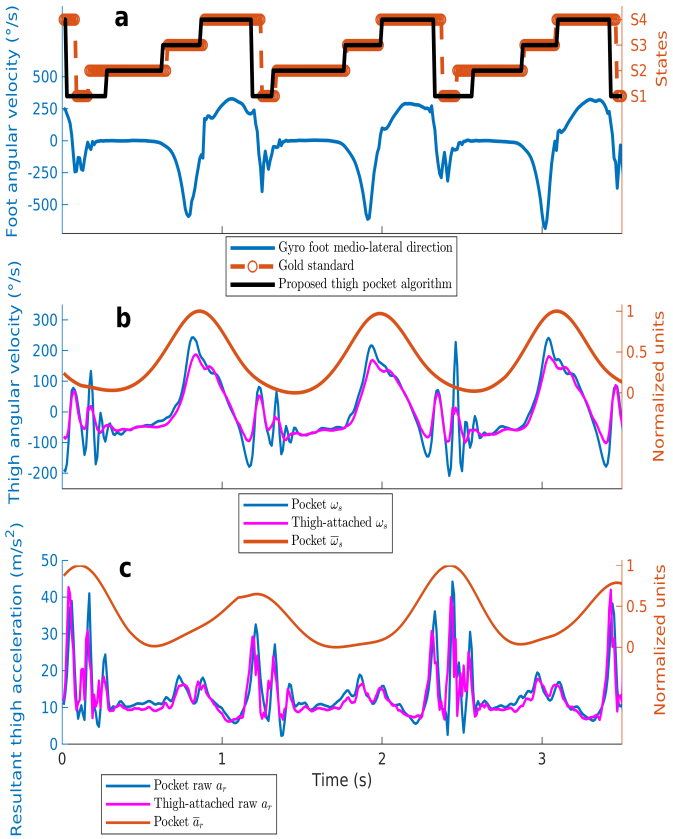

Fig. 4. Example results of the proposed algorithm in comparison to the gold standard (**a**) and thigh signals - sagittal angular velocity (**b**) and resultant acceleration (**c**) - acquired from a thigh-attached and an in-the-pocket IMU. Angular velocity is positive when the leg is going forward. The left axes correspond to the raw signals. On **b** and **c**, the right axis show the pocket signals after the filtering and adaptive normalization processes described in section IV, marked with an upper-bar on the legend. They are part of the proposed observation vector. The peak of $\overline{\omega}_s$ corresponds to the rule-based detection of TO.

VIII. Results

Fig. 4 presents example results from the gait event detection along with raw outputs from the pocket and thigh-attached IMUs. It also shows processed signals utilized in our algorithm.

A. Algorithms from the literature

Table III shows the $F1$-Scores and MSEs obtained by different algorithms at different IMU placements. The algorithms from [4], [9], [16] performed well, having obtained median $F1$-Scores ≥ 0.876 for all events. The algorithm by Piriyakulkit [16], although designed for an IMU placed on an assistive device on the side of the thigh, achieved a good performance using an IMU in the thigh pocket. Of note, in

TABLE III
PERFORMANCE OBTAINED FOR EACH ALGORITHM AT DIFFERENT IMU PLACEMENTS

		Foot-mounted (n=9)	Shank-attached (n=8)*	Thigh-attached (n=9)	Thigh pocket with simulated smartphone noises (n=9)		
		[9] HMM $[\tilde{\omega}_s]$** Eval. 1	**HMM $[\tilde{\omega}_s]$** Eval. 1	**HMM $[\overline{\omega}_s]$** Eval. 1	**Proposed HMM-RB $[\overline{\omega}_s, \overline{\omega}_r, \overline{a}_r]^T$** Eval. 1	Eval. 2	Eval. 3
$F1$-Score	HS	0.996 [0.982 1.000]	0.961 [0.856 0.996]	0.995 [0.986 0.997]	0.987 [0.952 0.994]	0.930 [0.769 0.986]	0.964 [0.910 0.990]
	FF	0.996 [0.983 1.000]	0.910 [0.751 0.991]	0.949 [0.793 0.994]	0.955 [0.878 0.991]	0.797 [0.553 0.946]	0.757 [0.594 0.909]
	HO	0.996 [0.982 1.000]	0.954 [0.832 0.991]	1.000 [0.987 1.000]	0.996 [0.990 1.000]	0.986 [0.921 0.997]	0.995 [0.973 1.000]
	TO	0.997 [0.983 1.000]	0.964 [0.856 0.997]	0.000 [0.000 0.570]	0.997 [0.992 1.000]	0.995 [0.981 1.000]	0.997 [0.989 1.000]
	MSE	0.051 [0.040 0.075]	0.173 [0.133 0.259]	0.327 [0.265 0.382]	0.169 [0.126 0.218]	0.350 [0.252 0.517]	0.282 [0.240 0.340]
		[9] (RB)	**[4] (RB)**	**[16] (RB)**	**[16] (RB)**	**HMM $[\overline{\omega}_s]$** Eval. 1	**HMM-RB $[\overline{\omega}_r, \overline{a}_r]^T$** Eval. 1
$F1$-Score	HS	1.000 [0.995 1.000]	0.997 [0.974 1.000]	0.900 [0.521 0.987]	0.876 [0.801 0.923]	0.994 [0.981 0.997]	0.801 [0.423 0.888]
	FF	1.000 [0.995 1.000]	-	-	-	0.914 [0.461 0.990]	0.828 [0.701 0.922]
	HO	1.000 [0.992 1.000]	-	-	-	1.000 [0.991 1.000]	0.881 [0.785 0.950]
	TO	1.000 [0.995 1.000]	0.989 [0.953 1.000]	0.935 [0.527 0.990]	0.929 [0.870 0.958]	0.735 [0.030 0.972]	0.920 [0.848 0.979]
	MSE	0.025 [0.017 0.036]	-	-	-	0.968 [0.359 1.621]	0.412 [0.323 0.537]

Results shown as median [Q1 Q3] (lower and upper quartiles). Observation vectors used for HMMs are shown in brackets. n: number of subjects, ω_s: sagittal angular velocity, ω_r: resultant angular velocity, a_r: resultant linear acceleration. As defined in section IV, filtered signals are marked with a tilde, while signals filtered and adaptively normalized are marked with an upper-bar. *One of the subjects did not carry the shank IMU. **Our implementation does not include the heuristic strategy in [9] which ignores strides lasting less than 0.35 s.

the original work of Piriyakulkit, the parameters were tuned for each subject, while here we used the same parameters for all subjects (given in Supplementary Appendix), which were tuned until good results were achieved for a single subject.

B. Pure HMMs

Pure HMMs (decoded by the standard Viterbi algorithm, without additional rule) performed well for the foot and shank locations (median $F1$-Scores $\geq$ 0.910 for all events). The MSE of the pure HMMs using a single input increased in the following order of sensor placement: foot, shank, thigh-attached and thigh pocket. For the thigh-attached and pocket locations, the performance of TO detection was poor (median $F1$-Scores of 0.000 and 0.735, respectively). This illustrates our motivation to design the TO-Rule.

C. HMM-RB algorithm using an IMU in the thigh pocket with simulated smartphone noises

Here we present the results for the proposed HMM-RB approach (observation vector $[\overline{\omega}_s, \overline{\omega}_r, \overline{a}_r]^T$ and TO-Rule verified on $\overline{\omega}_s$).

In Eval.1, the lower quartile $F1$-Scores were $\geq$ 0.878 and median $F1$-Scores were $\geq$ 0.955 for all events. In Eval. 2 and Eval. 3, the lower quartile $F1$-Scores for HS, HO and TO events were $\geq$ 0.769 and median $F1$-Scores were $\geq$ 0.930, while for FF the $F1$-Scores were 0.797 [0.553 0.946] and 0.757 [0.594 0.909], respectively. The TO-Rule detected the TO event robustly, having obtained a lower quartile of the $F1$-Score $\geq$ 0.981 in all evaluation types. The raw results for all walking sessions for all repetitions for all evaluation types are shown in Supplementary Fig. S1.

Applying the same approach but using the observation vector $[\overline{\omega}_r, \overline{a}_r]^T$ and verifying the TO-Rule on $\overline{\omega}_r$, lower performances were achieved in Eval. 1 in comparison to the proposed observation vector. Lower quartile $F1$-Scores were 0.423 and median $F1$-Scores were $\geq$ 0.801 for all events. This was an attempt to develop an orientation-free algorithm, since in this case all inputs are resultant quantities.

Table IV shows the time agreement (median [Q1 Q3]) between the proposed HMM-RB $[\overline{\omega}_s, \overline{\omega}_r, \overline{a}_r]^T$ algorithm and the gold standard. Positive delays mean that the algorithm detected an event after the gold standard. Only TP are considered. The proposed algorithm showed a bias towards detecting HS in advance (median delay of -30 ms in Eval. 1) and FF after the gold standard (median of 40 ms in Eval. 1). HO and TO showed small delays (medians of -10 ms and 00 ms in Eval. 1, respectively). The normalized frequency distributions of the delays between the events detect by the algorithm and the gold standard for each evaluation type are shown in Supplementary Fig. S2. Only TP are considered.

TABLE IV
DELAYS BETWEEN ALGORITHM AND GOLD STANDARD

	Delays [ms] (median [Q1 Q3])			
ET	HS	FF	HO	TO
Eval. 1	-30 [-80 10]	40 [00 80]	-10 [-40 10]	00 [-30 20]
Eval. 2	-40 [-110 50]	-10 [-100 90]	00 [-70 60]	-10 [-30 20]
Eval. 3	-40 [-110 20]	40 [-80 120]	-10 [-60 50]	-10 [-30 20]

ET: Evaluation type.

IX. DISCUSSION

Our goal was to develop an algorithm capable of detecting four gait events (HS-FF-HO-TO) using a single IMU in the thigh pocket, because this is a common carrying position of a smartphone. Instead of acquiring directly the signals from the smartphone's IMU, we attached to it a high quality Xsens IMU, which captured the smartphone's movements. We then added simulated noises to the pocket IMU to mimic the signal quality of a smartphone MEMS IMU. This experimental setup was designed to overcome problems in the acquisition of smartphone signals that could interfere on the quality of the measurements, and therefore, on the reliability of the algorithm

validation. Notably, IMUs from smartphones may be hard to synchronize with a gold standard and may have unstable/low sampling frequencies. We consider that the setup was suitable to validate our algorithm.

The results were promising and comparable to previous algorithms in the literature designed for positions known to achieve high performances, such as the (foot, shank and thigh)-attached IMU locations. [13] obtained F1-Scores $\geq$ 0.94 for the classification of four gait phases from thigh kinematics using high precision motion capture system. Our algorithm also showed better performances for the HS and TO detection in comparison to [16] when using the IMU in the thigh pocket with simulated smartphone noises. Due to the lack of algorithms in the literature for smartphone-based gait segmentation it is difficult to further compare our results. In light of the results from the three types of evaluation, we observed that our algorithm had a high generalization capability, given that our data was highly variable with respect to walking speeds. These results pave the way for future work which may evaluate the performances using signals directly from smartphones. Monitoring the evolution of patients in rehabilitation treatment and detection of neurological diseases are potential future applications of algorithms that consider an IMU/smartphone in the thigh pocket.

This work has limitations. The performances were evaluated in a small number of subjects with no gait abnormalities. Usually the performances decrease in impaired subjects [14]. Also, instead of the usual gold standards, we considered a set of rules using a foot-mounted IMU as our reference. These rules are not perfect, despite being an improved version of rules previously utilized in the literature as a surrogate for gold standard. If usual gold standards such as motion capture system were available, we would have used them in our study.

Although we aimed to use resultant quantities (ω_r and a_r) as input signals, our method is not completely orientation-free because the sagittal angular velocity ω_s was also used both for the observation vector and for the TO-rule. This requires the sensitivity axis of the gyroscope to be oriented in the medio-lateral direction so that ω_s is positive when the leg is going forward. Depending on the sizes of the pocket and of the IMU/smartphone, the orientation of the sensors may change over time, possibly causing distribution shifts in their outputs. Moreover, changes in walking speed cause changes in the signals' amplitudes and waveforms. The adaptive normalization was an attempt to solve the distribution shift issue and the results were satisfactory. We also applied our algorithm to an observation vector containing only resultant quantities but the performance decreased.

The method was implemented in post-processing, but some modifications could allow an online implementation. It would be necessary to use the online Viterbi algorithm [45]. The TO-rule would have to be verified in the forward direction, not backwards as in our modified backtracking. Moreover, it would be necessary to design online filters for each of the signals. The adaptive normalization would have to be implemented in a causal window.

Our method could also be used in a system designed to help the identification of diseases or estimate the degree of gait impairment. The detailed knowledge of gait phases given by our method has not yet been seen in the literature of smartphone-based gait analysis and it is relevant because it opens new possibilities for clinical applications. To test these applications, clinical trials would be required. For example, patients with intermittent claudication may have a prolonged flat-foot [29] phase, which previous smartphone-based gait segmentation algorithms cannot identify. For such an application, an implementation in post-processing as here would be the most adequate. The raw smartphone signals could be sent to the cloud where they would be processed and then a report would be later provided to the user, after acquisition of large amounts of data that wouldn't be available on a real-time implementation. One possible source of interference and artifacts in our method is when the user is performing other activities rather than walking. To avoid this, here we identified the beginning and end of each walking session manually. To detect and isolate them automatically on a dataset containing several daily-life activities, it would be necessary to implement an activity recognition algorithm capable of identifying the walking sessions, such as those presented in [21].

X. Conclusions

We proposed an adaptive Hidden Markov Model/Rule-Based algorithm to detect four gait events using a single IMU in the thigh pocket. The IMU was attached to a smartphone to capture the smartphone's movements in the pocket. We added simulated noises to the pocket IMU to mimic the signal quality of MEMS IMUs found in smartphones. The approach was evaluated in nine subjects with no gait abnormalities. Our algorithm using the pocket IMU demonstrated high performances, comparable to other algorithms in the literature for IMUs attached to the body or to assistive devices. This work is a step towards allowing accurate and refined gait segmentation from a smartphone carried in the pocket during daily activities.

Data Availability Statement

An example of populational model matrices can be obtained from the corresponding author upon reasonable request. The data from the experiments is not available since gait data potentially contains identifying information.

References

[1] U. Givon, G. Zeilig, and A. Achiron, "Gait analysis in multiple sclerosis: Characterization of temporal-spatial parameters using GAITRite functional ambulation system," *Gait and Posture*, vol. 29, no. 1, pp. 138–142, 2009.

[2] H. T. T. Vu, D. Dong, H. L. Cao, T. Verstraten, D. Lefeber, B. Vanderborght, and J. Geeroms, "A review of gait phase detection algorithms for lower limb prostheses," *Sensors (Switzerland)*, vol. 20, no. 14, pp. 1–19, 2020.

[3] J. Taborri, E. Palermo, S. Rossi, and P. Cappa, "Gait partitioning methods: A systematic review," *Sensors (Switzerland)*, vol. 16, no. 1, pp. 40–42, 2016.

[4] J. K. Lee and E. J. Park, "Quasi real-time gait event detection using shank-attached gyroscopes," *Medical and Biological Engineering and Computing*, vol. 49, no. 6, pp. 707–712, 2011.

[5] S. Miyazaki, "Long-term unrestrained measurement of stride length and walking velocity utilizing a piezoelectric gyroscope," *IEEE Transactions on Biomedical Engineering*, vol. 44, no. 8, pp. 753–759, 1997.

[6] Jacquelin Perry MD, *Gait analysis: normal and pathological function*, 1st ed. SLACK Incorporated, 1992.

[7] R. Caldas, M. Mundt, W. Potthast, F. Buarque de Lima Neto, and B. Markert, "A systematic review of gait analysis methods based on inertial sensors and adaptive algorithms," *Gait and Posture*, vol. 57, no. February, pp. 204–210, 2017. [Online]. Available: http://dx.doi.org/10.1016/j.gaitpost.2017.06.019

[8] A. Mannini, V. Genovese, and A. M. Sabatini, "Online decoding of hidden markov models for gait event detection using foot-mounted gyroscopes," *IEEE Journal of Biomedical and Health Informatics*, vol. 18, no. 4, pp. 1122–1130, 2014.

[9] A. Mannini and A. M. Sabatini, "A hidden Markov model-based technique for gait segmentation using a foot-mounted gyroscope," *Proceedings of the Annual International Conference of the IEEE Engineering in Medicine and Biology Society, EMBS*, pp. 4369–4373, 2011.

[10] J. C. Prez-Ibarra, A. A. G. Siqueira, and H. I. Krebs, "Identification of Gait Events in Healthy and Parkinson's Disease Subjects Using Inertial Sensors: A Supervised Learning Approach," *IEEE Sensors Journal*, vol. 20, no. 24, pp. 14 984–14 993, 2020.

[11] A. Mannini and A. M. Sabatini, "Accelerometry-based classification of human activities using Markov modeling," *Computational Intelligence and Neuroscience*, 2011.

[12] J. D. Farah, N. Baddour, and E. D. Lemaire, "Design, development, and evaluation of a local sensor-based gait phase recognition system using a logistic model decision tree for orthosis-control," *Journal of NeuroEngineering and Rehabilitation*, vol. 16, no. 1, pp. 1–11, 2019.

[13] ——, "Gait phase detection from thigh kinematics using machine learning techniques," *2017 IEEE International Symposium on Medical Measurements and Applications, MeMeA 2017 - Proceedings*, pp. 263–268, 2017.

[14] J. C. Pérez-Ibarra, H. Williams, A. A. Siqueira, and H. I. Krebs, "Real-Time Identification of Impaired Gait Phases Using a Single Foot-Mounted Inertial Sensor: Review and Feasibility Study," *Proceedings of the IEEE RAS and EMBS International Conference on Biomedical Robotics and Biomechatronics*, vol. 2018-Augus, pp. 1157–1162, 2018.

[15] J. C. Prez-Ibarra, A. A. Siqueira, and H. I. Krebs, "Real-Time Identification of Gait Events in Impaired Subjects Using a Single-IMU Foot-Mounted Device," *IEEE Sensors Journal*, vol. 20, no. 5, pp. 2616–2624, 2020.

[16] S. Piriyakulkit, Y. Hirata, and H. Ozawa, "Real-time gait event recognition for wearable assistive device using an IMU on thigh," *2017 IEEE International Conference on Cyborg and Bionic Systems, CBS 2017*, vol. 2018-January, pp. 314–318, 2017.

[17] D. Quintero, D. J. Villarreal, D. J. Lambert, S. Kapp, and R. D. Gregg, "Continuous-Phase Control of a Powered Knee-Ankle Prosthesis: Amputee Experiments Across Speeds and Inclines," *IEEE Transactions on Robotics*, vol. 34, no. 3, pp. 686–701, 2018.

[18] D. J. Villarreal, H. A. Poonawala, and R. D. Gregg, "A Robust Parameterization of Human Gait Patterns Across Phase-Shifting Perturbations," *IEEE Transactions on Neural Systems and Rehabilitation Engineering*, vol. 25, no. 3, pp. 265–278, 2017.

[19] W. Hong, N. Anil Kumar, and P. Hur, "A Phase-Shifting Based Human Gait Phase Estimation for Powered Transfemoral Prostheses," *IEEE Robotics and Automation Letters*, vol. 6, no. 3, pp. 5113–5120, 2021.

[20] J. Lee, W. Hong, and P. Hur, "Continuous Gait Phase Estimation Using LSTM for Robotic Transfemoral Prosthesis across Walking Speeds," *IEEE Transactions on Neural Systems and Rehabilitation Engineering*, vol. 29, pp. 1470–1477, 2021.

[21] M. Straczkiewicz, P. James, and J. P. Onnela, "A systematic review of smartphone-based human activity recognition methods for health research," *npj Digital Medicine*, vol. 4, no. 1, pp. 1–15, 2021.

[22] M. B. del Rosario, S. J. Redmond, and N. H. Lovell, "Tracking the evolution of smartphone sensing for monitoring human movement," *Sensors (Switzerland)*, vol. 15, no. 8, pp. 18 901–18 933, 2015.

[23] M. Gadaleta and M. Rossi, "IDNet: Smartphone-based gait recognition with convolutional neural networks," *Pattern Recognition*, vol. 74, pp. 25–37, 2018. [Online]. Available: http://dx.doi.org/10.1016/j.patcog.2017.09.005

[24] H. Zhang, C. Xu, H. Li, A. S. Rathore, C. Song, Z. Yan, D. Li, F. Lin, K. Wang, and W. Xu, "PDMove: Towards Passive Medication Adherence Monitoring of Parkinson's Disease Using Smartphone-based Gait Assessment," *Proceedings of the ACM on Interactive, Mobile, Wearable and Ubiquitous Technologies*, vol. 3, no. 3, pp. 1–23, 2019.

[25] P. Silsupadol, K. Teja, and V. Lugade, "Reliability and validity of a smartphone-based assessment of gait parameters across walking speed and smartphone locations: Body, bag, belt, hand, and pocket," *Gait and Posture*, vol. 58, no. September, pp. 516–522, 2017. [Online]. Available: http://dx.doi.org/10.1016/j.gaitpost.2017.09.030

[26] R. Altilio, A. Rossetti, Q. Fang, X. Gu, and M. Panella, "A comparison of machine learning classifiers for smartphone-based gait analysis," *Medical and Biological Engineering and Computing*, vol. 59, no. 3, pp. 535–546, 2021.

[27] J.-M. Paquet, B. Auvinet, D. Chaleil, and E. Barrey, "Analysis of gait disorders in parkinson's disease assessed with an accelerometer," *Revue neurologique*, vol. 159, no. 8-9, p. 786789, September 2003. [Online]. Available: http://europepmc.org/abstract/MED/13679722

[28] I. Bylemans, M. Weyn, and M. Klepal, "Mobile phone-based displacement estimation for opportunistic localisation systems," *3rd International Conference on Mobile Ubiquitous Computing, Systems, Services, and Technologies, UBICOMM 2009*, pp. 113–118, 2009.

[29] L. N. Gommans, A. T. Smid, M. R. Scheltinga, E. Cancrinus, F. A. Brooijmans, K. Meijer, and J. A. Teijink, "Prolonged stance phase during walking in intermittent claudication," *Journal of Vascular Surgery*, vol. 66, no. 2, pp. 515–522, 2017. [Online]. Available: http://dx.doi.org/10.1016/j.jvs.2017.02.033

[30] N. Abhayasinghe and I. Murray, "Human Gait Phase Recognition Based on Thigh Movement Computed using IMUs," *IEEE Ninth International Conference on Intelligent Sensors, Sensor Networks and Information Processing (ISSNIP)*, April 2014.

[31] S. Šprager and M. B. Jurič, "Robust stride segmentation of inertial signals based on local cyclicity estimation," *Sensors (Switzerland)*, vol. 18, no. 4, 2018.

[32] L. R. Rabiner, "A Tutorial on Hidden Markov Models and Selected Applications in Speech Recognition," *Proceedings of the IEEE*, vol. 77, no. 2, pp. 257–286, 1989.

[33] K. Murphy, *Hidden Markov Model (HMM) Toolbox for Matlab*, 1998. [Online]. Available: https://www.cs.ubc.ca/ murphyk/Software/HMM/hmm.html

[34] C. Angeloni, P. O. Riley, and D. E. Krebs, "Frequency Content of Whole Body Gait Kinematic Data," *IEEE Transactions on Rehabilitation Engineering*, vol. 2, no. 1, pp. 40–46, 1994.

[35] S. Jayalath and I. Murray, "A Gyroscope Based Accurate Pedometer Algorithm," *International Conference on Indoor Positioning and Indoor Navigation*, p. 31, October 2013.

[36] T. Oberg, A. Karsznia, and K. Oberg, "Basic gait parameters: Reference data for normal subjects, 10-79 years of age," *Journal of Rehabilitation Research and Development*, vol. 30, no. 2, pp. 210–223, 1993.

[37] S. Al-Obaidi, J. C. Wall, A. Al-Yaqoub, and M. Al-Ghanim, "Basic gait parameters: A comparison of reference data for normal subjects 20 to 29 years of age from Kuwait and Scandinavia," *Journal of Rehabilitation Research and Development*, vol. 40, no. 4, pp. 361–366, 2003.

[38] J. Borenstein and L. Ojeda, "Heuristic reduction of gyro drift in vehicle tracking applications," *International Journal of Vehicle Information and Communication Systems*, vol. 2, no. 1-2, pp. 78–98, 2009.

[39] M. Narasimhappa, A. D. Mahindrakar, V. C. Guizilini, M. H. Terra, and S. L. Sabat, "An improved Sage Husa adaptive robust Kalman Filter for de-noising the MEMS IMU drift signal," *2018 Indian Control Conference, ICC 2018 - Proceedings*, vol. 2018-January, no. Icc, pp. 229–234, 2018.

[40] N. El-Sheimy, H. Hou, and X. Niu, "Analysis and modeling of inertial sensors using allan variance," *IEEE Transactions on Instrumentation and Measurement*, vol. 57, no. 1, pp. 140–149, 2008.

[41] J. A. Farrell, F. O. Silva, F. Rahman, and J. Wendel, "IMU Error Modeling Tutorial: INS state estimation with real-time sensor calibration." *IEEE Control System Magezine*, 2021. [Online]. Available: https://escholarship.org/uc/item/1vf7j52p

[42] W. Yan, Q. Zhang, L. Wang, Y. Mao, A. Wang, and C. Zhao, "A modified kalman filter for integrating the different rate data of gyros and accelerometers retrieved from android smartphones in the gnss/imu coupled navigation," *Sensors (Switzerland)*, vol. 20, no. 18, pp. 1–17, 2020.

[43] S. Sirikonda and L. Parayitam, "Integration of low-cost IMU with MEMS and NAVIC/IRNSS receiver for land vehicle navigation," *Proceedings of the 34th International Technical Meeting of the Satellite Division of the Institute of Navigation, ION GNSS+ 2021*, no. October, pp. 2705–2717, 2021.

[44] H. T. T. Vu, F. Gomez, P. Cherelle, D. Lefeber, A. Nowé, and B. Vanderborght, "ED-FNN: A new deep learning algorithm to detect percentage of the gait cycle for powered prostheses," *Sensors (Switzerland)*, vol. 18, no. 7, 2018.

[45] R. Sramek, "The on-line Viterbi algorithm," Master's thesis, Department of Computer Science Faculty of Mathematics, Physics and Informatics Comenius University, Bratislava, 2007.

Francisco A. Garcia is currently a Ph.D. researcher at Katholieke Universiteit Leuven, Belgium. He received his B.E. in Electrical Engineering from the University of São Paulo, Brazil and his Master's Degree from Supélec, France. He received the Best Students Award in 2020 from Instituto de Engenharia, Brazil. His research interests include computational modelling, machine-learning and signal processing applied to manufacturing and healthcare.

Juan C. Pérez-Ibarra received the B.E. degree in electronics engineering from the Universidad de los Llanos, Villavicencio, Colombia, in 2010; and the M.S. and Ph.D. degrees in mechanical engineering from the University of São Paulo at São Carlos, Brazil, in 2014 and 2019, respectively. From 2017 to 2018, he was a Graduate Visiting Student with the MIT's Department of Mechanical Engineering. From 2019 to 2021 he was a Post-Doctoral Associate with the Department of Electrical Engineering, University of São Paulo at São Carlos, Brazil. He is currently a Post-Doctoral Fellow of the Department of Mechanical and Aerospace Engineering at the University of California, Irvine, USA. His research interests include gait analysis, biomechanics, robotic rehabilitation, and control systems.

Marco H. Terra received the Ph.D. degree in electrical engineering from the University of São Paulo (USP), São Carlos, Brazil, in 1995. He is currently a Full Professor in electrical engineering with USP. He has reviewed articles for over 30 journals and to the Mathematical Reviews of the American Mathematical Society. He has authored over 260 conference papers and journal articles. He has co-authored the book Robust Control of Robots: Fault-Tolerant Approaches (Springer). His research interests include filtering and control theories, fault detection and isolation problems, and robotics. He was the Coordinator of the Robotics Committee and the President of the Brazilian Automation Society. He is also an Ad Hoc Referee for the Research Grants Council of Hong Kong. He is also the Coordinator of the Brazilian Institute of Science and Technology for Cooperative Autonomous Systems Applied to Security and Environment.

Adriano A. G. Siqueira received the bachelor's degree in mechanical engineering and the Ph.D. degree in electrical engineering from the University of São Paulo, São Paulo, Brazil, in 1999 and 2004, respectively. Since 2006, he is an Associate Professor with the Mechanical Engineering Department, São Carlos School of Engineering, University of São Paulo. In 2012, he took a sabbatical leave with the Massachusetts Institute of Technology. Since 2020, he is the head of the Center of Engineering Applied to Healthy. His research interests include robust control, $H\infty$ control, underactuated manipulators, fault tolerant systems, exoskeletons, and rehabilitation robotics.